Astron. Astrophys. 343, 10–18 (1999)

ASTRONOMY AND ASTROPHYSICS

Analysis of the OGLE microlensing candidates using the image subtraction method

C. Alard[1,2]

[1] DASGAL, Observatoire de Paris, 61 Avenue de l'observatoire, F-75014 Paris, France
[2] IAP, 91bis boulevard Arago, F-75014 Paris, France

Received 14 August 1998 / Accepted 29 October 1998

Abstract. The light curves of the OGLE microlensing candidates have been reconstructed using the image subtraction method. A large improvement in the photometric accuracy has been found in comparison with previous processing of the data with DoPHOT. In the mean, the residuals to the fit of a microlensing light curve are improved by a factor of 2 for baseline data points, and by a factor of 2.5 during magnification. The largest improvement was found for the OGLE #5 event, where we get an accuracy 7.5 times better than with DoPHOT. Despite some defects in the old CCD used during the OGLE I experiment, most of the time we obtain errors that are only 30% to 40% in excess of the photon noise. Previous experiment showed that with modern CCD chips (OGLE II), residuals much closer to the photon noise were obtained. The better photometric quality enabled us to find a low amplitude, long term variability in the OGLE #12 and OGLE #11 baseline magnitude. We also found that the shape of the OGLE #14 candidate light curve is quite inconsistent with microlensing of a point source by a point lens. A dramatic change in the light curve of the OGLE #9 candidate was also found, which indicates that very large biases can be present in data processed with DoPHOT. To conclude we made a detailed analysis of the blending issue. It is found that OGLE #5, OGLE #6 and OGLE #18 are very likely highly blended microlensing events. These events result from the magnification of a faint star that would have been undetectable without microlensing.

Key words: techniques: image processing – cosmology: dark matter – cosmology: gravitational lensing

1. Introduction

The ongoing microlensing surveys (OGLE, EROS, MACHO) are currently providing us with an enormous number of images of dense crowded stellar fields. These new data stimulated software development. Several successful implementations based on the DoPHOT software (Udalski et al. 1993 Bennet et al. 1992) have been used so far to extract the stellar magnitudes from the images. Other software, like PEIDA, which has been developed by the EROS group (Ansari et al. 1996) has also been used with some success. However, all these packages use the same basic profile fitting method to estimate the magnitudes of the stars present in the image. This method is not optimal in the case of microlensing surveys, as our aim is only to detect and measure variations. Purely differential methods, like the image subtraction technique should give better results. The recent release by the OGLE collaboration (Wozniak & Szymanski 1998) of a collection of small images centered on each OGLE microlensing candidate, and the corresponding light curves, offers a nice opportunity to test this assumption. We will analyze these images with the method recently developed by Alard & Lupton (1998). This method is designed to give optimal results, and is well suited to small images, as all the pixels can be used to derive the best kernel solution. We will compare the image subtraction light curves with the light curves obtained by Wozniak & Szymanski (1998) using the DoPHOT software (Schechter et al., 1993).

Send offprint requests to: C. Alard

2. The subtracted images

We have a few hundred 101x101 images for each OGLE candidate. These OGLE I images show a mean quality that seems to be well below the quality of the OGLE II images (Udalski et al. 1997). A subsample of the OGLE II images has already been processed with the image subtraction method (Alard & Lupton 1998).

2.1. Image registration and re-sampling

As described in Alard and Lupton (1998), we register the images by fitting the positions of the brightest stars. For these small images, we used a polynomial transform of order 1. Each image is then transformed to the astrometric system of a reference image by using a bicubic spline interpolation. This procedure provides us with a collection of images that have the same sampling but different values of the seeing.

2.2. Building a reference for image subtraction

We found that better results are obtained if we derive a high quality and almost noise free reference image. We approach

this requirement by stacking between 10 and 20 of our best seeing (interpolated) images. Using this image, we also compute a "masked" image in which all obvious defects like saturated stars, or bad CCD regions, are masked by setting the relevant pixels in the reference frame to zero. The image subtraction program will use this masked image to derive the list of pixels that should not be fitted when deriving the kernel solution.

2.3. Image subtraction

As it has been already described in Alard & Lupton (1998), the core of the problem is to find a convolution kernel that will transform our reference frame to exactly the same seeing as another frame. To find the best kernel solution we have to solve a set of linear least-square equations. We keep the same general kernel decomposition that we already used for the OGLE II data. However, this time we modify the code in order to take into account the defects in the reference image. If we do not take this precaution, the convolution with the kernel would spread the defects and pollute the fit. To solve this problem the linear least square matrix is built by convolving the reference image with each of the vectors we use for the kernel decomposition. We do not wish to calculate the convolution at the pixels we have masked. But the problem will occur just at the border of the masked areas. To compute the convolution at a given position we need the values of the pixels all around this position, within some limiting radius. If some area around our position falls within the masked area we can not get any reasonable value for the relevant pixels. But we can find a straightforward solution to this problem by not using these pixels to calculate the convolution, and to compensate by re-normalizing the filter. We re-normalize the filter so that its sum over all the pixels we have not discarded is again one. There are however some convolution filters that have a zero sum. We solve this difficulty by splitting the filter into 2 different filters that do not have a zero sum. We processed the frames for all the OGLE candidates with this method, and we found that the treatment of the defects was very satisfactory.

2.4. Quality of the subtracted images

For some of the subtracted images we get residuals that are consistent with the Poisson fluctuations. However for a large number of frames we found some systematic residual patterns which seems to be related to the behavior of some of the CCD columns. We also found that the residuals associated with most of the bright stars were very satisfactory, showing that we reached a good kernel solution, but some showed systematics for one of the bright stars (somewhat in excess of the Poisson fluctuation). As a consequence of these defects the photon noise limit which we easily reached with OGLE II data (Alard & Lupton 1998) is not as clearly reached in the case of these OGLE I data. The same image subtraction software has also been used for EROS data (Afonso et al. 1998), and as in the case of OGLE II the residuals were in good agreement with the photon noise.

3. Photometry of the subtracted images

In the first paper concerning this image subtraction method, we used an easy and straightforward way to estimate the flux in each subtracted image. Our aim was not to produce the best quality light curves, but just to show consistency with the photon noise. We estimated the total flux by taking all the flux in a large aperture radius. This is of course not optimal. A better way to proceed is to make aperture photometry in a small radius only, and to compute an aperture correction. It is also possible to use a generic profile fitting technique, by assuming that the profile is a bi-dimensional gaussian that we fit for each image. However, some experiments show that the result is no better than using corrected aperture photometry. It is also important to point out that in the case of profile fitting photometry small biases are introduced by the fact that the analytical model for the profile never perfectly matches the real PSF. We make a differential correction for this bias by comparing the flux of bright stars calculated by profile fitting in the image to the flux we estimated in the reference image using the same method. The correction factor we derive this way is a few percent. To improve the photometry we need to derive a very accurate PSF model. This is not an easy task in very crowded fields.

3.1. Optimized photometry of the subtracted images

In this paper we do not derive an analytical model for the PSF. All we need to know is the PSF at the position of the variable star we want measure. We select a few bright stars in the image. Around each of these bright stars, we extract sub-images. We also extract a sub-image around the star we wish to measure. We then re-center the bright stars, so that their exact position in their sub-images is the same as the position of the measured star in its sub-image. For this re-centering we use bicubic splines. We emphasize that in order to get an unbiased position for the variable object (not the position of the nearest star), we stack all the subtracted images for which we find a significant signal at the location of the candidate. This way we build a high signal to noise image of the differential variations. We then use this image to estimate the center of the microlensing candidate. We also normalize each bright star sub-image by using a cross-product with a gaussian. We then do a median stacking of all sub-images, in order to get a numerical PSF bitmap. We use this PSF bitmap to estimate the flux in the relevant subtracted image. Of course, as we have already explained, we systematically apply the differential fitting correction, in order to get rid of small discrepancies in our PSF model; although this time the discrepancy is very small. This procedure gives the best results. We found a mean gain of about 20 to 30% in the accuracy of the photometry in comparison with the corrected aperture photometry. This indicates that most of the PSF's have very complicated shapes.

4. Fit of microlensing light curves to the data

In order to make a comparison between the light curves obtained with DoPHOT (Wozniak & Szymanski, 1998) and the

Table 1. Fit of microlensing light curves. We use the following notation: D/S is the ratio between DoPHOT residual and the image subtraction residual to the fit of a microlensing light curve. Chi2 is the square root of the Chi-square calculated by normalizing the residuals to the fit of the image subtraction light curve with the Poissonian deviation. We present this quantity because it gives directly the percentage of error in addition to the theoretical Poisson error. Additionally, the column Mag gives the DoPHOT magnitude corresponding to the baseline. The last 2 columns represent the percentage errors for the baseline and the magnification periods. The capital letter (A) is for during magnification data, and (B) is for data belonging to the baseline of the event. We also present the mean * quantity which is the mean of the various parameters calculated only for the candidates that are marked with a *.

Candidate	D/S (B)	D/S (A)	Chi2 (B)	Chi2 (A)	Mag	% (B)	% (A)
OGLE #1*	2.17	2.38	1.15	1.09	18.7	2.7	1.9
OGLE #2*	1.37	1.87	1.55	2.03	19.1	4.9	4.1
OGLE #3*	2.58	1.82	1.62	2.17	15.9	0.4	0.5
OGLE #4*	2.65	3.39	1.15	1.08	19.2	2.2	2.3
OGLE #5*	2.71	7.57	1.33	1.89	18.0	1.1	1.1
OGLE #6*	2.3	4.7	1.56	1.57	18.1	2.1	2.4
OGLE #8*	1.73	1.34	1.29	1.37	17.8	1.1	1.1
OGLE #9*	1.48	1.47	1.32	0.99	19.2	4.8	3.1
OGLE #11	1.09	1.45	1.60	1.47	18.1	2.4	1.9
OGLE #12	1.21	1.52	1.92	1.29	18.6	4.1	2.5
OGLE #14	1.76	1.46	1.40	3.11	19.0	2.9	4.4
OGLE #15*	2.93	3.17	1.23	1.69	18.3	3.4	2.8
OGLE #16*	1.71	1.36	1.19	1.46	18.4	1.0	1.0
OGLE #17*	1.74	1.92	1.26	1.55	18.7	3.0	2.2
OGLE #18*	1.61	2.14	1.40	1.37	18.6	2.5	1.8
OGLE #19*	1.72	2.99	1.48	0.92	19.7	4.9	2.7
Mean	1.96	2.5	1.4	1.56	18.5	2.7	2.2
Mean *	2.15	2.84	1.35	1.51	18.4	2.4	1.9

Note: For OGLE #19, Chi2 (A) = 0.92, but we have only a few points during magnification for this microlensing event.

image subtraction method, we fitted theoretical microlensing light curves to both sets of data. In the fitted parameters we include the blending parameter, as blending of these faint sources is likely. To make the comparison as accurate as possible, we selected the data points that were both in the DoPHOT and the image subtraction light curves. Some images were defective and they were not in the DoPHOT light curve. In the case of image subtraction almost all the frames were used. In very few cases, for instance when a saturation spike originating from a bright star came across the star image, we were unable to estimate the flux using this method. We had no problem processing very bad seeing images with the image subtraction method.

4.1. Analysis of the Chi-square and residuals to the fit

To make comparison of DOPHOT and image subtraction errors, we re-scaled each data set by dividing by the amplitude. We estimate this amplitude as the difference between the base line value and the value of the fitted curve at the location of the data point that shows the maximum magnification. We have also analyzed the consistency of the image subtraction errors with the Poisson noise. For this particular task we calculated the Chi-square of the distribution, by summing the square of the errors weighted with the Poisson (or photon noise) deviation. The Poisson deviation is estimated by calculating the variance of our magnitude estimator. In this calculation we assume that the Poisson distribution is well approximated by a Gaussian distribution with $\sigma = \sqrt{(counts/adu\_to\_el)}$ (adu_to_el is the conversion from ADU to electrons). The results obtained are summarized in Table 1. We see that the mean improvement we get with the image subtraction method is about a factor of 2 in comparison to DoPHOT. It seems we gain even more if we compare the residuals during the magnification phase. Thus it is clear that a dramatic improvement is obtained by using the image subtraction method. Additionally, most of the time we get errors that are only 10% to 40% in excess of the photon noise expectation. Some candidate events have errors considerably larger than the rest, and they introduce some biases in the mean value of the improvement; we will discuss this issue later.

To illustrate the improvement that we get by using the image subtraction method we present 3 different cases. First we present an event with mean improvement, for which the residuals are smaller by a factor of 2 (OGLE #1, Fig. 1). In the second figure we present the data for a case of a modest improvement (OGLE #2), the residuals are smaller by only 37% for the baseline and by 87% during the magnification. However, looking at the light curve, we see that the improvement is very significant. In particular, there are 2 bad seeing points at the top of the light curve that deviate a lot in the DoPHOT, but have much smaller errors in the image subtraction light curve. This well illustrates the ability of the method to deal with large seeing variations. Concerning the residuals along the baseline, it is important to note that at least one point has a very large deviation, which is not consistent with Poisson statistics. We must emphasize again

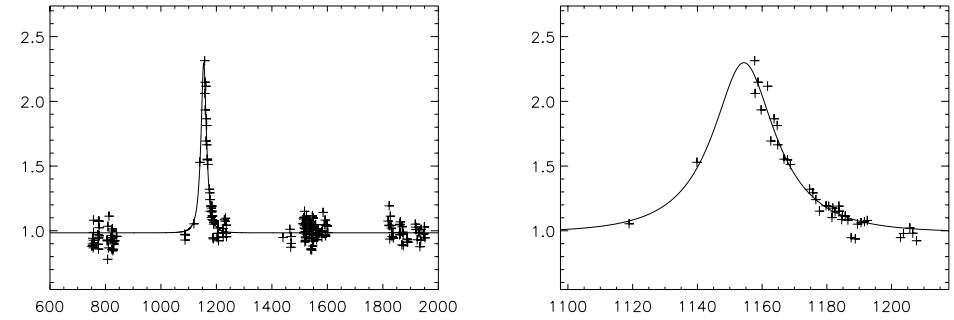

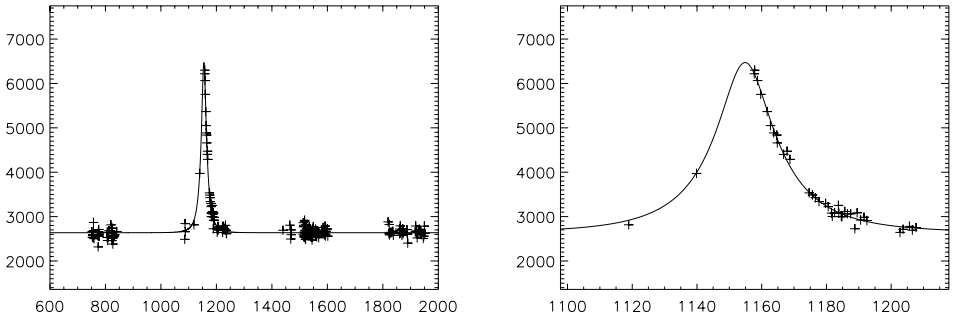

Fig. 1. OGLE #1 light curves. The *upper* light curves were obtained with DoPHOT, the *lower* with the image subtraction method. The latter improves the residual by a bit more than a factor of 2.

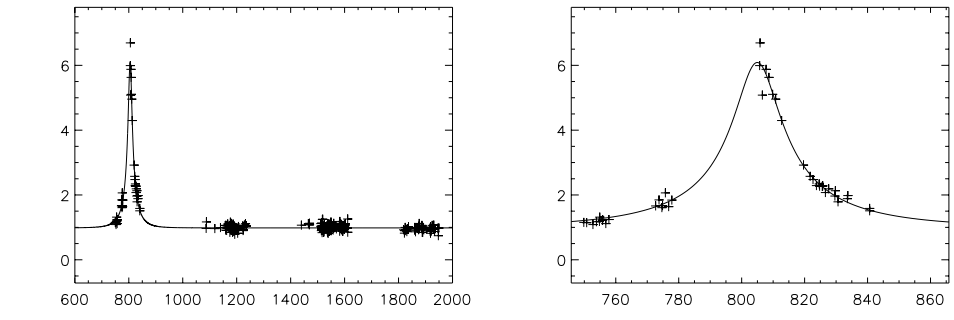

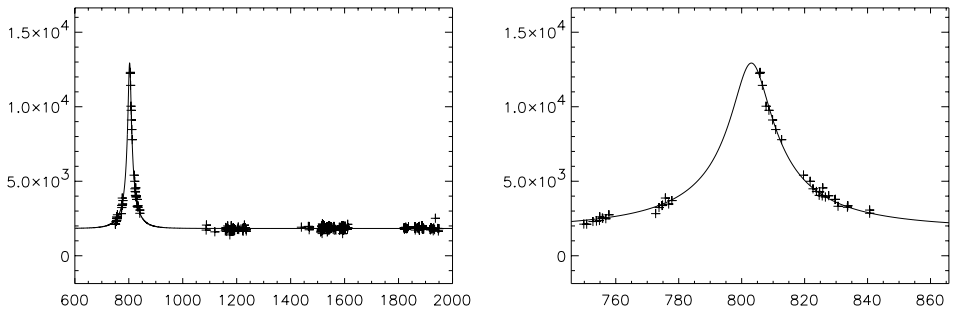

Fig. 2. OGLE #2 light curves. The *upper* light curves were obtained with DoPHOT, the *lower* with the image subtraction method. Note the spread for the 2 bad seeing points at top of the DoPHOT light curve. The image subtraction method reduces considerably the scatter of these bad seeing points.

that the CCD used during the OGLE I project had lot of defects and that might contribute to the errors.

To conclude, we present an example of a large improvement (OGLE #4), and a very large improvement (OGLE #5, Fig. 3). In the case of OGLE #4 the residuals are reduced by a factor 2.65 during the baseline and 3.4 during the magnification. It is important to note that this result has been obtained despite especially bad image quality for this event, and yet we get a Chi-square that is very close to the photon noise expectation. For OGLE #5, the residuals are reduced by a factor 7.5 during the magnification. This shows that the image subtraction method can lead to very dramatic improvement. This huge improvement can probably be explained by the fact that OGLE #5 is a case of an unresolved (highly blended) source (Alard 1997).

4.2. Light curves with large deviations from photon noise

The largest value of the Chi-square is for the OGLE #3 event. It is important to note that OGLE #3 is also the brightest of the candidates, and that it might indicate that there is a problem with the OGLE I data reaching the photon noise limit for bright stars. Considering that a typical photometric error is only $\sim 0.5\%$,

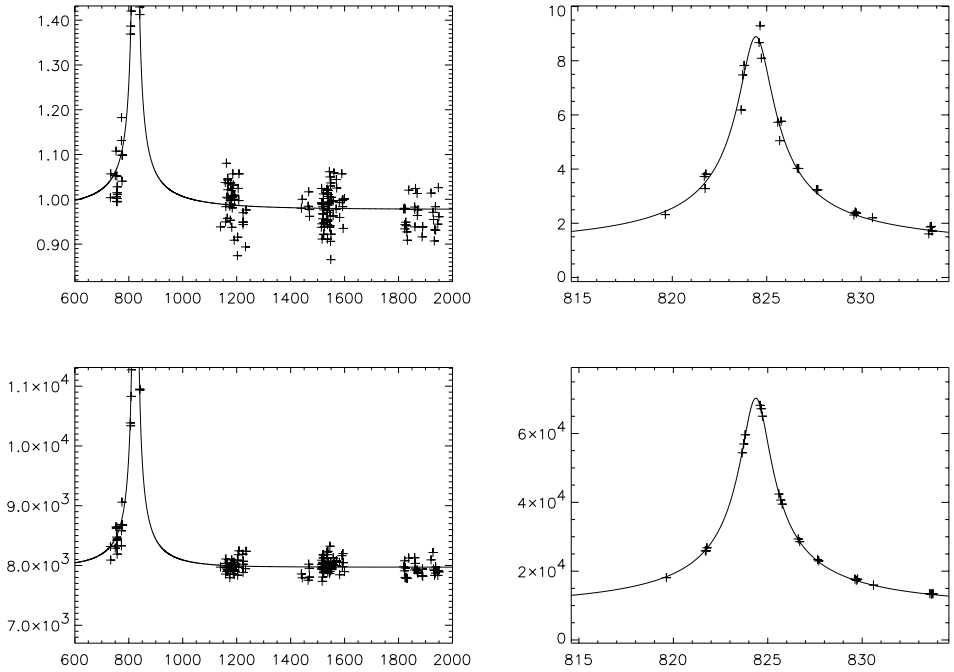

Fig. 3. OGLE #5 light curves. The *upper* light curves were obtained with DoPHOT, the *lower* with the image subtraction method. The residuals are improved by more than a factor of 7 during the magnification, this is the largest improvement obtained by using image subtraction.

any errors in the flat fielding may contribute to the global error budget. The problem may also be related to the quality of the CCD chip, and in particular to the stability of the PSF at the level of 1%. The analysis of subtracted images shows residuals with different shapes even for the bright stars that are quite close to each other. These differences cannot be explained by the seeing variations as the exposure time (10 min) is relatively long. We did not found such problems in our analysis of OGLE II data (Alard & Lupton 1998). To conclude the discussion on OGLE #3, it is important to emphasize that even if the image subtraction is a bit far from the photon noise deviation expected from our profile fitting method, it is about 2 times better than DoPHOT.

There are some faint stars that show large baseline residuals. These are: OGLE #2, OGLE, #11, OGLE #12, OGLE #14. In the case of OGLE #2 we get a bad Chi-square for both baseline and magnification data. The case of OGLE #11 and OGLE #12 is different, since Chi-square is bad during the baseline only. Finally, OGLE #14 is the most peculiar since it shows a very bad Chi-square during the magnification only.

It was not possible to find any reason for the bad Chi-square obtained for OGLE #2. The residuals do not show any systematics, and no periodic signal could be identified. It appears that OGLE #2 is quite different from the other OGLE events, since it lies close to the edge of the CCD. Considering the poor quality of this CCD this situation might lead to additional errors, especially in the flat fields.

The cases of OGLE #11 and OGLE #12 appear to be completely different since we can observe systematic patterns in the residuals (Figs. 4 and 5.). In the case of OGLE #12, it is clear that a systematic trend of the baseline magnitude is observed. A similar trend is also visible in the DoPHOT light curve, although it is less clear; it is also less reliable, as the image subtraction is purely differential and free of systematics. For OGLE #11 we also observe a systematic deviation of a clump of points near the date 1200. This seems to indicate that these 2 candidates have long term variations which resemble the variations observed for the OGLE #10 candidate (cf. Fig. 6). To conclude on the case of OGLE #11 and OGLE #12 it is interesting to note that Zebrun (1998) in his study of the long term variables in the OGLE fields identified a number of variables which have light curves resembling the baseline variations we observe. This may indicate a link to some type of variable star.

The OGLE #14 candidate does not show much deviations during the baseline, but it shows very significant deviations from the best fit during the magnification. In particular, a group of points near the tip of the descending branch shows a large systematic deviation. There is also a point which shows large deviations both, in the image subtraction and DoPHOT light curves. However the image corresponding to this data point does not show any particular defect, and seems to be of good quality. We conclude that the most likely explanation is that OGLE #14 could be a variable star, possibly a cataclysmic star, since we do not have a point on the rising branch that could eliminate this type of a variable. Another possibility would be that OGLE #14 is a case of lensing by a binary source, or lensing of a binary source. However with the current data set it is difficult to study this possibility.

These 4 microlensing candidates are also those which show the smallest improvements with the image subtraction method. This is not surprising, since it seems that in this case there is some additional error or intrinsic variability that the image subtraction can't improve. There is another case where the improvement due to image subtraction is rather small, this is the candidate OGLE #9. However, the DoPHOT light curve and the image subtraction light curve are very different (see Fig. 8), and

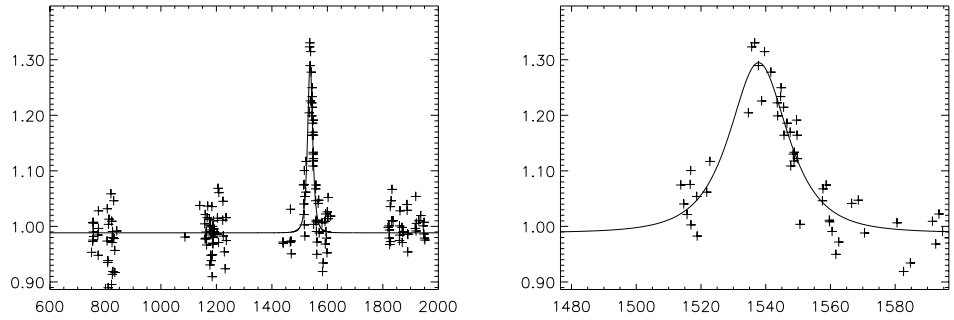

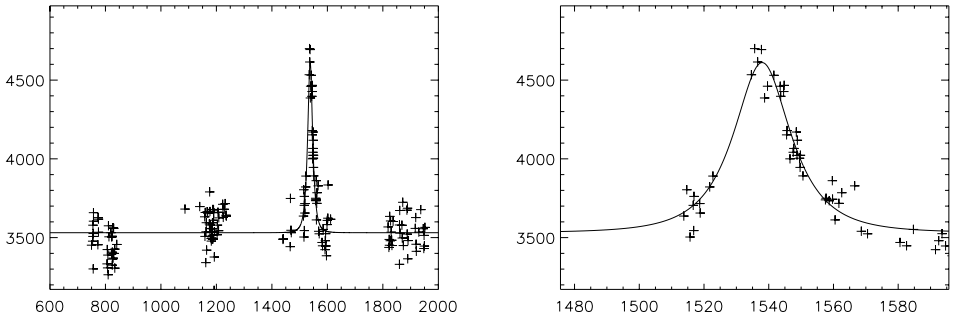

Fig. 4. OGLE #11 light curves. The *upper* light curves were obtained with DoPHOT, the *lower* with the image subtraction method. Note that in the image subtraction light curve, the clump of points near epoch 800 is slightly below the baseline on the mean, and that the clump of points near epoch 1200 is above the baseline. Due to larger errors, these features are hardly visible in the DoPHOT light curve.

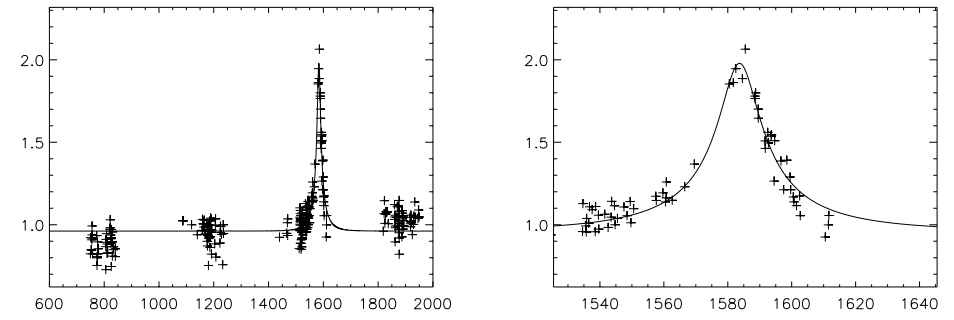

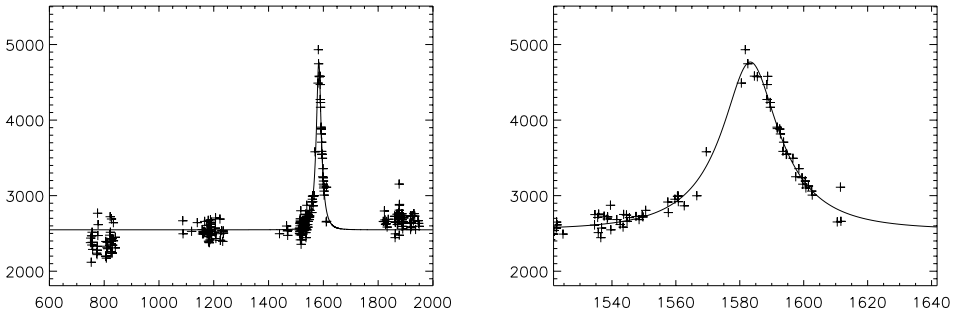

Fig. 5. OGLE #12 light curves. The *upper* light curves were obtained with DoPHOT, the *lower* with the image subtraction method. Note the rise of the mean baseline magnitude in both, DoPHOT and image subtraction light curves. The difference between the 2 edges of the baseline is about 0.2 magnitudes.

we wonder if the DoPHOT and the image subtraction measured exactly the same object. Looking at the composite reference image, we see that in the region occupied by OGLE #9 there are many very faint unresolved objects, and that some confusion is likely. Sometimes DoPHOT may find 1 or 2 objects, depending on the seeing.

To conclude this discussion, in Table 1, we present the mean of the residual ratios and the Chi-square when the 4 previous OGLE candidates are rejected. As it seems that for these 4 candidates additional (uncontrolled) errors or variations are present, it is difficult to derive a reliable statistics from them.

5. Blending analysis

In crowded fields blending of the source with fainter stars is likely (classical blending), and this possibility needs to be investigated. However another kind of blending is also possible, if the source is very faint and unresolved and it is seen only during the magnification (Alard 1997, Han 1997). This kind of microlensing events is likely to give an important contribution to the optical depth, and it is important to try to detect them. The task should be easer than in the case of classical blending, as the blending of the source is very large and it should make a

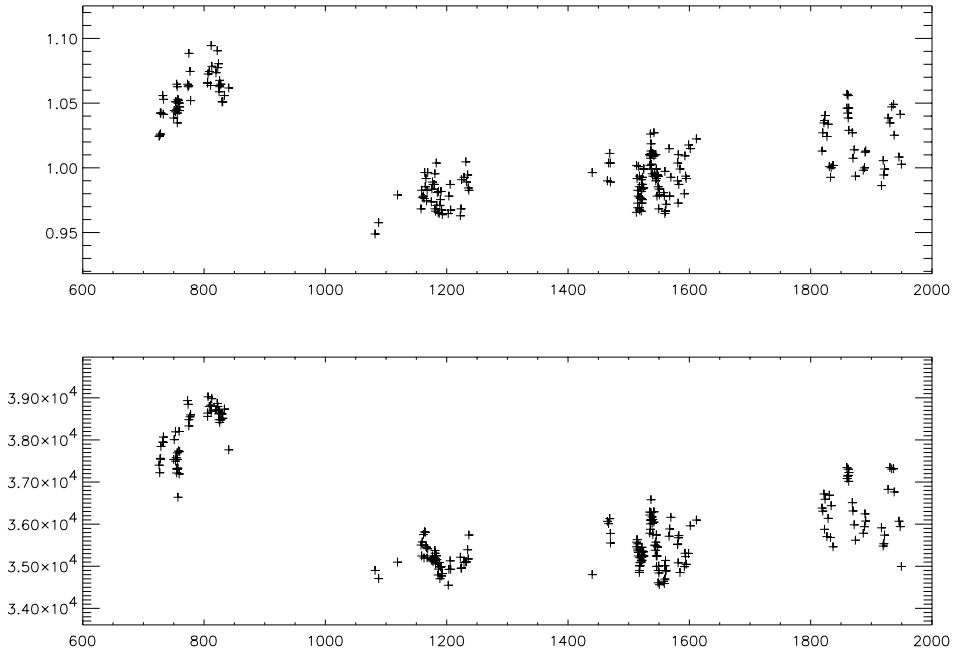

Fig. 6. OGLE #10 light curves. Up is DoPHOT, below the light curve obtained with the image subtraction method.

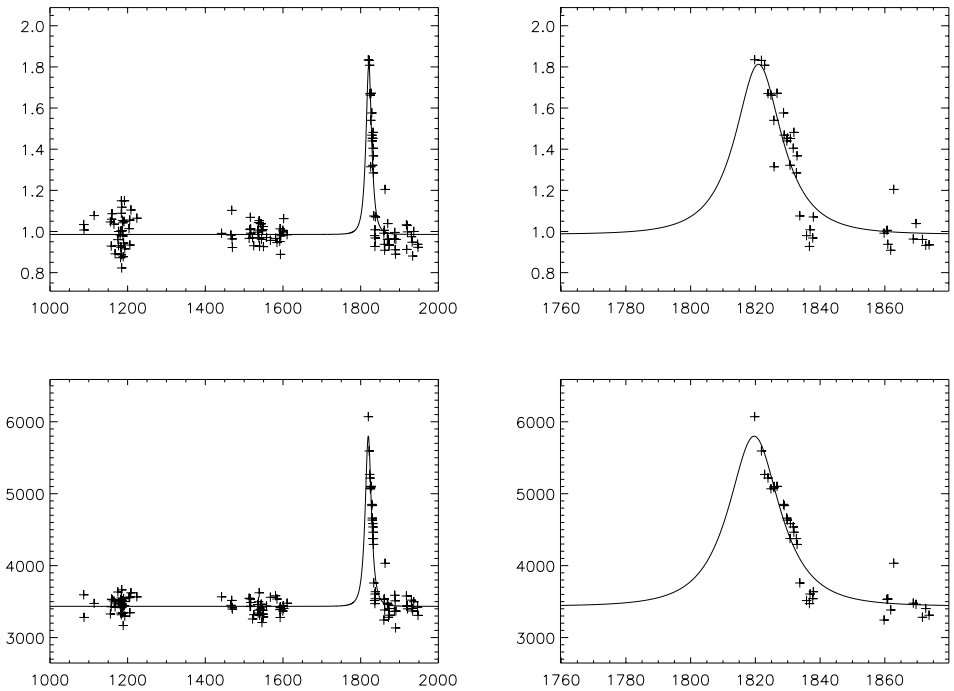

Fig. 7. OGLE #14 light curves. The *upper* light curves were obtained with DoPHOT, the *lower* with the image subtraction method. Note the clump of the systematicly deviating points at the tip of the decending branch in the image subtraction light curve. Also, note the deviating point near epoch 1860 in, both DoPHOT and image subtraction light curve.

more noticeable modifications of the light curve. To investigate the blending issue we need to get the baseline magnitude of the star associated with the variations. For this particular task, we used the median PSF model that we derived previously to fit the magnitude of the star on the reference image. For this PSF fitting we used the coordinates that were found for the variable by stacking the subtracted images.

5.1. Fit of models with and without blending to the light curves

To investigate the possibility of blending of the source, a solution with and without blending parameter, has been fitted to the image subtraction data, for each of the OGLE candidate. To compare the Chi-square's to the fit of the unblended and blended model, the F-test was performed, in order to estimate the significance of adding a blending parameter to the model. The result is presented in Table 2. It appears immediately that OGLE #5, OGLE #6, and OGLE #18 are blended microlensing events. Considering the flux ratio of the source to the flux of the resolved source, it is also very likely that these 3 events result from a large magnification of a faint unresolved star. OGLE #5 had already be identified as a lensing of an unresolved star with the previous OGLE data (Alard 1997), but the detection

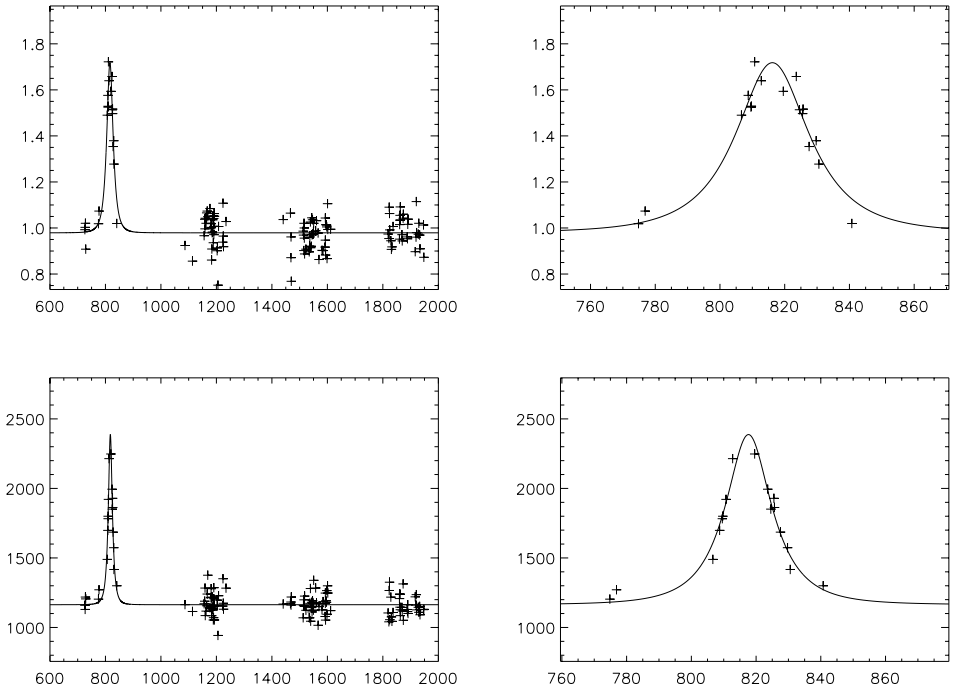

Fig. 8. OGLE #9 light curves. The *upper* light curves were obtained with DoPHOT, the *lower* with the image subtraction method. Note a completely different shape of the light curve obtained with image subtraction. This example shows that large biases can be present in the DoPHOT processed data. Image subtraction not only improves the photometric accuracy, but it also eliminates most biases.

Table 2. Blending analysis. In the first column we present the probability that adding a blending parameter to the fitted microlensing model is significant. In column 2 we give the flux ratio between the source (derived from fitting the blending parameter) and the associated star. In column 3 we give the magnitude of the source that has been calculated by applying the flux ratio correction to the DoPHOT baseline magnitude. For comparison purpose we also give the impact parameter and the Einstein ring crossing time in columns 4 and 5. Considering the large degeneracy of the solution in case of large blending factor, we also give the product $U_{min} \times t_0$ which is not affected by the degeneracy of the solution (Wozniak & Paczyǹski 1997)

Candidate	Probability	Blending ratio	Mag (I band)	U_{min}	t_0	$U_{min} \times t_0$
OGLE #1	0.644	1.6	21.8	0.3030	27.87	8.44
OGLE #2	0.559	1.3	19.3	0.1135	56.78	6.44
OGLE #3	0.500	1.0	15.9	1.1370	11.85	13.47
OGLE #4	0.781	1.6	19.7	0.1880	13.26	2.49
OGLE #5	1.000	25.0	21.4	0.0044	185.28	0.81
OGLE #6	1.000	10.1	20.6	0.0197	45.04	0.88
OGLE #8	0.541	1.3	18.0	0.5299	48.06	25.46
OGLE #9	0.500	1.0	19.2	0.5254	13.93	7.31
OGLE #11	0.501	1.5	18.5	0.8518	12.95	11.03
OGLE #12	0.528	2.1	19.4	0.3664	23.53	8.62
OGLE #14	0.500	1.0	19	0.7028	12.41	8.72
OGLE #15	0.500	1.0	18.3	0.1021	19.08	1.94
OGLE #16	0.605	4.4	20.0	0.4515	34.47	15.56
OGLE #17	0.500	1.0	18.7	0.5452	123.52	67.34
OGLE #18	0.999	11.2	21.2	0.0632	33.52	2.11
OGLE #19	0.671	2.6	20.7	0.0732	7.46	0.54

of OGLE #6 and OGLE #18 as very blended events is new. We emphasize that the confidence of detection of the blended nature of OGLE #5 has been greatly improved with the image subtraction method.

5.2. Comparison with the astrometric shift method

In this section we make a comparison with the analysis of astrometric shifts of the OGLE microlensing candidates performed by Goldberg & Wozniak (1998). Our 3 very blended events, OGLE #5, OGLE #6, and especially OGLE #18 all show very large astrometric shifts. In particular, the largest shift observed by Goldberg & Wozniak is for the OGLE #18 event. This confirms the prediction by Han (1998) and Goldberg (1998) that lensing of very faint highly blended objects should result in the observation of large astrometric shifts. On the other hand, some large astrometric shifts can be detected without any photometric evidence for them if the separation between the components is

large and the amplified star is not much fainter than the other blend component. When the separation between the blend components is small and the source is faint compared to the other component, then photometric analysis is a good way to detect blending. This shows that the two techniques are complementary.

6. Conclusion

This re-analysis of the OGLE images clearly demonstrates, with overwhelming evidence, the usefulness of the image subtraction method. On the average, we noticed an improvement by a factor of 2 in the photometric accuracy in comparison to DoPHOT. An improvement of ~ 2.5 was found for the data points taken during the magnification. This makes it possible to refine the interpretation of the OGLE microlensing candidates. The case of the strongly blended events, OGLE #5, OGLE #6, and OGLE #18 are especially important for further interpretations of the microlensing optical depth towards the Galactic Bulge (Alard 1997, Han 1997). OGLE #9 is also very interesting, as it shows a light curve that is completely different from the DoPHOT light curve. It is a good illustration of the large biases that might be present in data processed with DoPHOT. However, it was also found that small amplitude long term variations were present in the OGLE #12 and OGLE #11 baseline magnitudes. It is difficult to say if these variations make these 2 candidates inconsistent with microlensing. Further investigation should be conducted in order to estimate the likelihood of such variations in similar stars, which are either solar type or subgiants.

The case of OGLE #14 is more problematic since we have very significant evidence that the shape of the light magnification differs from that predicted for point-source microlensing. Since we have no data point on the rising branch, it is difficult to prove that this candidate is related to cataclysmic variables. It would be valuable to obtain a spectrum of the star in order to search for specific emission lines.

It is important to emphasize that the improvement provided by the image subtraction method should not be considered only in the case of producing individual light curves of selected objects. This method is well suited for global processing of all the microlensing data. Due to the fact that the whole linear least-square matrix has to be built only once for the reference image, the computing time of the method is very reasonable and should compete with DoPHOT. To conclude, we would like to emphasize that the improvement that has been found in the quality of the light curves is not in any sense specific to OGLE. This testing has been conducted with OGLE data, as OGLE has been the first to provide massive release of images. However such similar improvements, have already been found for the light curves of 2 microlensing candidates obtained with EROS data (e.g. Afonso et al., 1998), and it will certainly be seen for other microlensing data-set, as all these projects use DoPHOT or DoPHOT like softwares. It is also important to add that some small photometric effects which were not found with DoPHOT (see OGLE # 12 for instance), will probably also be found when large data-sets from the other microlensing experiments are analyzed with the image subtraction method.

The light curves of all OGLE microlensing events can be accessed with anonymous ftp at: ftp.iap.fr, directory: pub/from_users/alard/ogle.

Acknowledgements. The author would like to thank all the OGLE team for public release of the image data-set. Without this unique opportunity, accurate testing of the new image subtraction method, and comparison with previous method would have been impossible. It is a pleasure to thank B. Paczyński, P. Wozniak and D. Goldberg for their kind help and comments. Finally, I would like to thank R. Catchpole for reading this manuscript.

References

Afonso C., et al., 1998, A&A 337, L17 (astro-ph/9806380)
Alard C., Lupton R.H., 1998, ApJ 503, 325 (astro-ph/9712287)
Alard C., 1997, A&A 326, 1
Ansari R., 1996, Vistas in Astronomy. 40, 519
Bennett D., 1992, Texas/PASCO, International Conference, Berkeley, CA, 13-18 Dec. 1992
Goldberg D.M., 1998, ApJ 498, 156
Goldberg, D.M., Wozniak P., 1997, Acta Astron. 48, 19 (astro-ph/9712262)
Han C., 1997, ApJ 490, 51
Han C., 1998, astro-ph/9804272
Schechter P., Mateo M., Saha A., 1993, PASP 105, 1342
Udalski A., Kubiak M., Szymanski M., 1997, Acta Astron. 47, 319 (astro-ph/9710091)
Udalski A., et al., 1993, Acta Astron. 43, 69
Wozniak P., Paczyǹski B., 1997, ApJ 487, 55
Wozniak P., Szymanski M., 1998, Acta Astron. 48, 269 (Astro-ph/9804193)
Zebrun, 1998, Acta Astron. 48, 289